Unbalanced Distribution Network Cross-Country Fault Diagnosis Method with Emphasis on High-Impedance Fault Syndrome

Balamurali Krishna Ponukumati

School of Electrical Engineering, KIIT Deemed to be University, India
pbmk20031993@gmail.com (corresponding author)

Anil Kumar Behera

School of Electrical Engineering, KIIT Deemed to be University, India
anil.beherafel@kiit.ac.in

Lipsa Subhadarshini

School of Electrical Engineering, KIIT Deemed to be University, India
lipsa.subhadarshinifel@kiit.ac.in

Pampa Sinha

School of Electrical Engineering, KIIT Deemed to be University, India
pampa.sinhafel@kiit.ac.in

Manoj Kumar Maharana

School of Electrical Engineering. KIIT Deemed to be University, India
mkmfel@kiit.ac.in

Arapirala Venkata Pavan Kumar

Department of EEE, Madanapalle Institute of Technology & Science, India
pawanrao82@gmail.com

ABSTRACT

Unusual fault scenarios can occur on the utility grid in a power system network. Cross-Country Faults (CCFs) connected to the High-Impedance Fault (HIF) syndrome are more prone to occur in forested areas due to thunderstorms, cyclones, and improper vegetation management and tree pruning. Finding and categorizing CCFs associated with HIF syndrome is a great challenge. This study employed the cross-correlation method to reconstruct the signals produced by CCFs with HIF, which were shown to be complicated, aperiodic, asymmetric, and nonlinear. A decreased sensitivity to random noise means that a given modification might not affect equally all component peaks. This allows for more precise signal recovery. The maximum voltage cross-correlation coefficients were carefully evaluated as distinguishing elements in the development of a suggested fault detection technique. The proposed concept was evaluated on a modified imbalanced IEEE 240 bus system under different case studies. These case studies cover a wide range of scenarios, such as the switching of a capacitor bank, feeder energization, and the effects of nonlinear loads under noisy conditions.

Keywords-Cross Country Faults (CCF); High Impedance Fault (HIF); cross-correlation; slime mould optimization technique; non-negative matrix factorization; method of peak detection

I. INTRODUCTION

The Cross-Country High Impedance Fault (CCHIF) can be described as "high-impedance ground faults happening in separate phases of one circuit at different places at the same time as the fault inception time" in a typical scenario. The main challenges in cross-country faults in transmission/distribution systems are the detection of distance, direction, and phase selection. These faults are simultaneous or evolving problems in the network. The relay may experience failure to function correctly in cases where there is an internal issue within its designated zone or may operate erroneously when a fault occurs outside it. This complexity arises from the unpredictable distribution of zero- and negative-sequence components along the protected line, which is used by the above mentioned functions. This unpredictability affects both solidly grounded systems and those that are either isolated or impedance grounded [1].

Wavelet Transform (WT) is a signal-processing technique that has been widely used for HIF detection [2]. Using a collection of filters, WT can analyze HIF signals at various resolution levels. Artificial Neural Networks (ANNs) and fuzzy expert systems, along with WT, have been employed to detect HIF in distribution networks [3-6]. In [7], a graph theory-based zone identification method and Random Search Multilevel Support Vector Machine (RSMSVM) algorithm were used to accurately categorize the fault zone. The moving sum approach and mathematical morphology [8-9] are different signal processing tools, and conventional relays can help detect HIFs. Ongoing research is focused on precise identification and location estimation of HIFs using methods such as evidential reasoning [10], parameter estimation [11], and computation of fault resistances [12].

In Unified Power Flow Controller (UPFC) compensated transmission lines, a backup protection technique based on differential apparent power can help the traditional distance protection system with HIF detection [13]. In [14], a signal-processing-based method was proposed to extract the necessary data to detect and locate HIF in the situation of a single line to ground fault, where the voltage and current signal were decomposed into orthogonal components. In [15], a method for identifying malfunctioning feeders in HIF was presented, considering the Peterson coil's influence. In [16], a single-phase composite power-based HIF protection approach for a low-resistance grounded distribution network was proposed, without considering the polarity of the current transformers. In [17-18], new models for the identification of HIFs were introduced. Nowadays, wind farms are gradually integrated into grids at various voltage levels. When a wind farm is connected to the grid through a transmission line, the voltage of the system constantly fluctuates, and as a result, fault classification becomes more intricate.

Recent studies have highlighted the growing use of Support Vector Machines (SVM) for power system fault monitoring. The SVM approach focuses on recognizing system faults, particularly power system instability, using bus voltages, times before and after faults, and generator angles as training data. A trained SVM effectively identified abnormal conditions after disturbance [19]. Other studies evaluated the impact of integrating wind power into the system, employing the Multi-Band Power System Stabilizer (MBPSS) to suppress dynamic oscillations. Simulations confirm MBPSS's ability to enhance system stability under severe faults and high integration of wind farms [20-21]. This study proposes a unique approach to identifying the location of an HIF fault zone in a distribution system. The innovative contributions of this study are:

- A cross-correlation-based scheme for identifying cross-country HIFs in the distribution system is proposed. The method involves analyzing the cross-correlation between the voltage under normal operating conditions and the voltage during a faulty state to identify distinctive characteristics in the signature.

- The correlogram as a useful tool for data analysis is validated by demonstrating its ability to reduce the effect of uncorrelated random noise. Feature extraction aims to create fresh features from the ones already present in a dataset, thereby decreasing the dataset's size. These refined features should succinctly encapsulate the meaningful information in the original features. Through the amalgamation of the initial features in this manner, a more concise rendition of the original set can be produced.

II. PROPOSED METHOD

A. Feature Extraction based on Time Cross-Correlation

A correlation describes how closely two variables are related. Correlation is helpful because it shows the connection between two variables, which enables users to forecast how a system will behave in the future. In simpler terms, cross-correlation serves as a statistical tool for assessing the extent to which two correlated signals resemble each other. The time series is expected to be organized chronologically with $I = 1$, ..., N. The periodogram is conventionally defined as the squared modulus of the Discrete Fourier Transform (DFT) and serves as an approximation for Power Spectral Density (PSD):

$$P(v_k) =$$
$$\frac{2T}{N^2}\left(\left[\sum_{i=1}^{N} f_i \cos(2\pi v_k t_i)\right]^2 + \left[\sum_{i=1}^{N} f_i \sin(2\pi v_k t_i)\right]^2\right) \text{(1.a)}$$

By applying normalization to the cross-correlation function, a Pearson correlation coefficient that is time-adjusted can be obtained:

$$\rho xx(t_1, t_2) = \frac{K_{xx}(t_1, t_2)}{\sigma x(t_1)\sigma x(t_2)} = \frac{E\left[(X_{t_1} - \mu_{t_1})\overline{(X_{t_2} - \mu_{t_2})}\right]}{\sigma x(t_1)\sigma x(t_2)} \quad \text{(1.b)}$$

Specifically, a stochastic process's normalized cross-correlation is defined as:

$$\rho xy(\tau) = \frac{K_{xy}(\tau)}{\sigma x \sigma y} = \frac{E\left[(X_t - \mu x)\overline{(Y_{t+\tau} - \mu y)}\right]}{\sigma x \sigma y} \quad \text{(1.c)}$$

$$Kx(\tau) = E[x(t1)y(t1 + \tau)] = E[x(t_1 - \tau)y(t_1)]$$
$$= E[y(t_1)x(t_1 - \tau)] = Ky(-\tau) \quad \text{(1.d)}$$

where μ_x is the mean and σ_y is the standard deviation of the processes X_t and Y_t, respectively, which are constant over time, and K_{xy} is the cross co-variance function respectively.

Frequencies are given by $v_k = k/T$, where k can be any integer from 1 to N, and $v_k = k/(N-1)/2$, where N is an odd number. The maximum frequency is the Nyquist frequency $v_{Nyq} = (N/2)(1/T)$, the minimum frequency is $v_{min} = 1/T$, and $T = N(t_N - t_1)/(N-1)$. The cross-correlation between 2 signals, $x(n)$ and $y(n)$ is given by:

$$\hat{R}_{xy}(m) = \begin{cases} \sum_{n=0}^{N-m-1} x_{n+m}y_n & m \geq 0 \\ \hat{R}_{yx}(-m) & m < 0 \end{cases} \qquad (2)$$

where m is equal to 2, 1, 0, 1, 2. Subscript xy denotes the order in which the two variables are associated, and index m denotes a parameter that shifts with time. The subscripts are arranged so that x precedes y to indicate how one sequence is moved concerning the other. Compared to the equal sampling scenario, the uneven sampling case's window function shapes can account for the significant red-noise leakage shown in the simulations and the increased noise. Using even sampling, standard Fourier analysis results can be recreated, complete with the well-established characteristics of window functions. In the case of representing noise, it can be written:

$$x(t) = A\cos(\omega t + \theta) \qquad (3)$$

where θ is a random variable, $y(t)$ represents noise, and $x(t)$ and $y(t)$ are uncorrelated functions. Then, the autocorrelation coefficient of $x(t)$ is $Rx(\tau) = \frac{A^2}{2}\cos\omega\tau$. $Ry(t)$ is the autocorrelation function of noise $y(t)$. $Ry(\tau)$ should be decaying in nature. Hence correlograms are decaying in. Consider:

$$Ry(\tau) = Y_0^2 e^{-\infty/\tau} \qquad (4)$$

After adding $x(t)$ and $y(t)$, it becomes:

$$z(t) = x(t) + y(t) \qquad (5)$$

$$Z = A\cos(\omega t + \theta) + noise$$

$$R_z(\tau) = Rx(z) + Ry(\tau), \qquad Y_0^2 >> \frac{A^2}{z} \qquad (6)$$

If $x(t)$ contains several frequencies or a small band of frequencies, this band can be recovered from the new signal $Z(t)$. In this study, the Source Separation Non-Negative Matrices (SSNMF) algorithm was used to remove the significant noise.

B. Reducing Noise

The SSNMF method is represented graphically by a sweep sequence of amplitude spectra. The Frequency-Following Response (FFR) can be more easily seen, and extra noise is eliminated from all recordings thanks to the SSNMF decomposition. The analysis involves examining the patterns of improvement in FFR and reduction in noise as the number of sweeps increases. A model was developed using an exponential curve fit. Pitch processing and neuroplasticity processes during signal interruptions are two possible uses of the SSNMF algorithm on the FFR signal [22]. The machine learning algorithm takes a non-negative input matrix A and uses it to learn and factorize a smaller matrix S, which serves as the spectral basis, and T, which serves as the information coding.

$$A_{ij} \approx (ST)_{ij} = \sum_{k=1}^n S_{ik}T_{kj} \qquad (7)$$

Here, i and j stand for elements across matrix A's initial (a flattened frequency-time vector) and secondary (a sequence of amplitude spectrograms) dimensions, respectively. Following this approach, FFR and noise were independently reconstructed, as shown in Figure 1, using the following formulas: multiply the input data matrix T by their respective S-T ratios, and then divide the result by the matrix T.

$$FFR = \frac{A(S_{FFR}T_{FFR})}{ST} \qquad (8)$$

$$Noise = \frac{A(S_{noise}T_{noise})}{ST} \qquad (9)$$

The following equation is used to outline the efficiency improvement in the FFR signal (i.e. working of the SSNMF method):

$$B(n) = B_{BS}e^{\left(-\frac{n}{\tau}\right)} + B_{DC} \qquad (10)$$

In this context, B represents the performance index, specifically FFR improvement, n is the total amount of sweeps for each signal, B_{BS} is the asymptotic amplitude of the fitted curve minus the direct current component, and the constant e represents Euler's mathematical constant (approximately 2.7182) and denotes the time constant of the fitted curve, indicating the number of sweeps required to reach 63% of the asymptotic amplitude. B_{DC} refers to the direct current component of the fitted curve, representing the overall elevation of the fitted curve. For noise reduction, an alternative model was employed, showing results that exhibited an increasing trend as the number of sweeps increased.

$$B(n) = B_{BS}e^{\left(-\frac{n}{\tau}\right)} + B_{DC}$$

$$FFR Enhancement =$$

$$0.254 * (e^{\left(-\frac{n}{555}\right)}) + 0.005 \qquad (11)$$

$$Noise Reduction form signal =$$

$$20.653 * (1 - e^{\left(-\frac{n}{290}\right)}) - 20.991 \qquad (12)$$
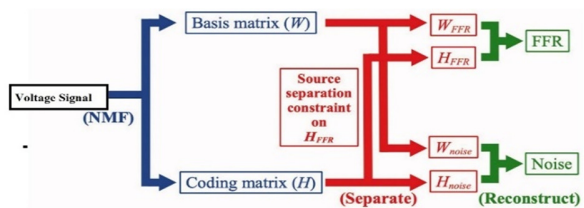
Fig. 1.   Block diagram of source separation using SSNMF algorithm.

C. Method of Peak Detection (MOPD) for Determining QRS

Applying Normal-Exponential-Bernoulli (NEB) and mixture probability models, a brand-new peak identification algorithm was used to analyze extensive two-dimensional electrical signals:

$$X_i \sim ND(\theta_i + \mu, \sigma^2) \text{ and } \theta_i \sim Exp(\phi) \qquad (13)$$

III. SYSTEM MODELING

A. Modified 240 Node System Modeling

This system consists of three feeders, as shown in Figure 2. Feeder A has 17 nodes, feeder B has 60 nodes, and feeder C has 162 nodes, all receiving power from a 69 kV substation. The major length of this distribution system is 23 miles, and it supplies electricity to more than 1100 people. Transformers are used for secondary supply clients. Real direct data on power consumption (kW) are available through smart meters at different locations based on the slime mould optimization technique. There are two capacitor banks in the 240-bus system. The substation features on-load tap changers at nodes 2038 and 3079. The introduction of photovoltaic (PV) systems at different locations alters this test system. As shown in Figure 2, a total of 20 PV systems were installed in the 240-node unbalanced distribution system. The size of the selected PV system size was 40 kVA, even if PV system sizes and locations are selected on a random basis using empirical data. Voltage readings are taken throughout the grid at various points.
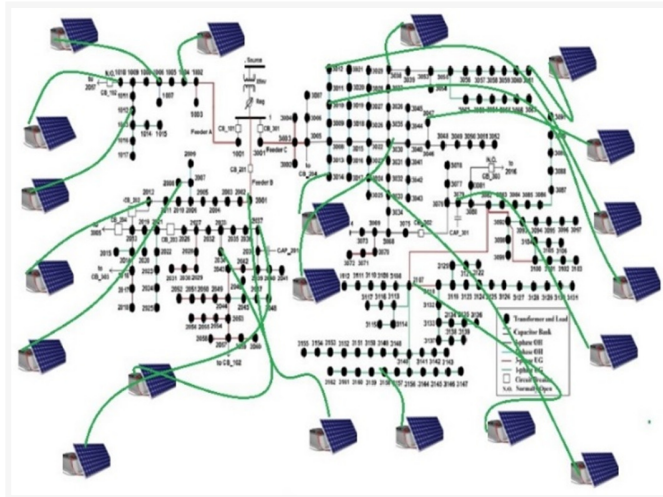
Fig. 2.   The IEEE modified 240 bus system.

B. HIF Modeling for Cross Country

A HIF exhibits traits similar to an electric arc, including non-linearity, inconsistency, and recurrence in the fault current signals. Additionally, these signals exhibit the existence of high-frequency components and harmonics. Various studies have proposed various HIF model types. This study considered a 2-diode HIF model, similar to [5]. The model consists of two DC voltage sources (V_p and V_n), two diodes (D_p and D_n), and two resistances (R_p and R_n) that are coupled in an antiparallel fashion. Asymmetric fault currents were produced in the distribution network using several sets of fault resistances R_p and R_n that have different values. When the line voltage is higher than the positive DC voltage (V_p), the fault current begins to flow in the direction of the ground. On the contrary, it returns from the ground when the line voltage is less than the negative DC voltage (V_n). If the phase voltage falls within the range of V_p and V_n, there is no fault current. This study considered three diverse situations built on three different

voltage and resistance values, as shown in Table I. Variation is necessary to achieve the various HIF behaviors and their effects on the electrical power distribution system [6]. When HIFs occur in a feeder, both negative and zero sequence currents are introduced. HIFs are mostly line-to-ground faults.

TABLE I.   HIF PARAMETERS

Sl. No.	HIF parameter values			
	V_p(V)	R_p (Ω)	V_n(V)	R_n (Ω)
Condition 1	3588	208	3847	212
Condition 2	6180	245	6155	245
Condition 3	8092	270	9358	290

IV. RESULTS AND DISCUSSION

To validate the proposed algorithm for the detection of cross-country HIFs, different capacitor bank switching feeder energization at various inception angles and locations were simulated, with both balanced and unbalanced loads as well as electronic power loads. The signal is generated at time $t = 0.1$ s with a sampling frequency of 2048 Hz, and the calculation is carried out one cycle after the fault event to determine the values of Q, R, and S. In this study cross-country-HIF and other transients were generated in the 240 bus distribution network on buses 1010, 1015, 2019, 2031, 3022, and 3035. Buses 1037, 1014, 1005, 1003, 1011, 1015, 2012, 2019, 2030, 2024, 2021, 2032, 2042, 2053, 2066, 2041, 2031, 3034, 3005, 3013, 3011, 3027, 3030, 3042, 3049, 3094, and 3067 are the best locations for the monitoring points, which were found using the slime mould optimization technique. At the measurement point, voltage signal correlation was tested under both normal and various transient conditions, such as cross-country faults. The two signals' cross-correlogram becomes their autocorrelation when everything is working properly. The cross-correlogram produces various waveforms for various types of transients. Figure 3 shows the extraction of features for CCHIF detection on bus 1010.
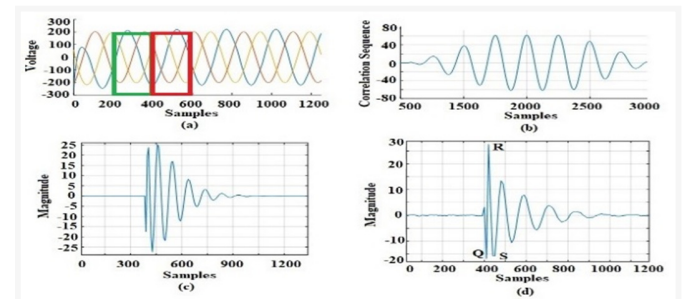
Fig. 3.   Extraction of features for CCHIF detection at bus 1010: (a) voltage signal during CCHIF, (b) correlation with pure signal, (c) signal after correlation and MOPD operation, and (d) signal after filtering.

Since there are two periodic switching fingerprints in two consecutive windows that do not overlap, they can be dismissed by subtracting the matching data from both windows. A technique based on cross-correlation is used to guarantee that the difference is small or zero under typical conditions. This is performed by calculating the cross-correlation of the windows at varying delays. The windows'

similarity is at its highest when the estimated cross-correlation value is maximized, and the windows' length is recalculated after taking into account the appropriate latency. This method guarantees that the subtraction of similar samples yields the correct result.

Figure 4 shows the correlograms for some example studies. The CCHIF correlogram under condition 3 in Figure 5(a) was generated at 0.02 s on bus 1010 and observed from bus 1013. Figure 4 (b, c) shows the correlograms of the capacitor bank switching and the feeder energization on bus 1015 at 0.02 s, respectively. Figure 5 shows that the *Q*, *R*, and *S* points are indistinguishable in scenario *c*. Therefore, the associated signal is subjected to MOPD action, followed by SSNMF operation to produce the waveforms shown in Figure 5. From this figure, three separate values can be obtained for *Q*, *R*, and *S*, which were used for CCHIF detection.
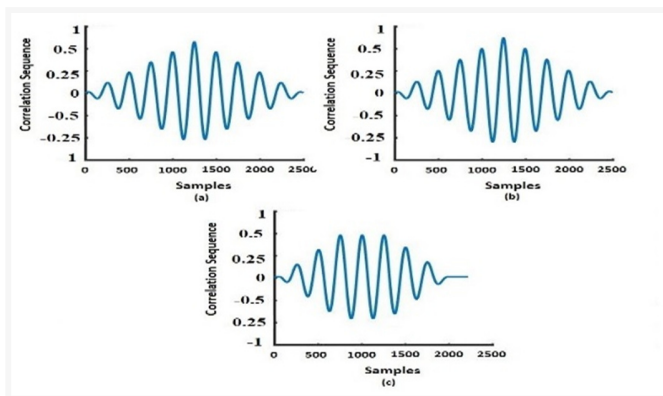
Fig. 4.   Cross-correlogram of CCHIF: (a) CCHIF, (b) switching of the capacitor bank, and (c) energization of the feeder.
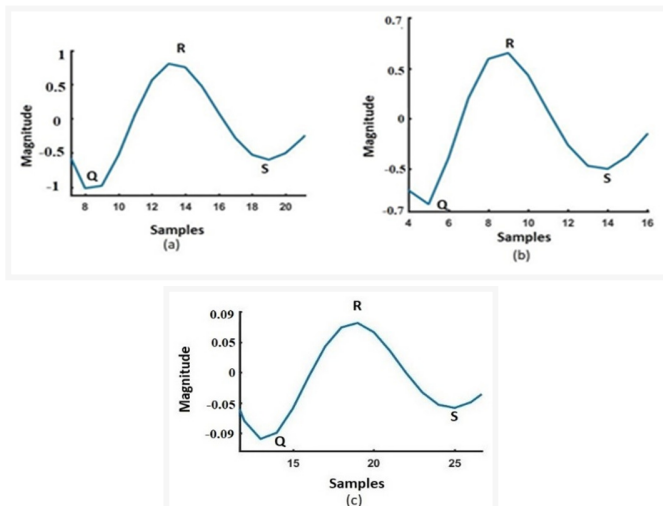
Fig. 5.   Cross-correlogram post MOPD and filter operation to obtain *Q*, *R*, and *S* points: (a) CCHIF, (b) signal for switching the capacitor bank.

V.   METHOD VERIFICATION UNDER DIFFERENT CONDITIONS

A. Influence of Noise

The voltage and current signals in real-time systems are always contaminated with noise. Unwanted electrical impulses that interfere or distort with an original (or desired) signal are known as noise or interference. As a result, the effectiveness of the suggested approach for cross-country HIF detection was investigated in noisy environments. The entire recorded signal contains power system noise, which has a normal probability distribution. The Signal-to-Noise Ratio (SNR) that states this noise, is given by:

$$SNR_{dB} = 20.log_{10}\left(\frac{A_{signal}}{A_{noise}}\right) \qquad (14)$$

B. CCHIF Fault Detection Influence of Power Electronics Load

Power electronics interfaced nonlinear loads, such as time-varying harmonics in distribution networks, are now widely employed by both home and industrial customers. The proposed solution was tested with a non-linear load to assess its performance. A 6-pulse converter bridge that provides a DC load of 650 kW at 3.6 kV and is coupled at various points of the 240-bus distribution network was used to design the non-linear load.

VI.   CONCLUSIONS

This study introduces a reliable correlation-based method for detecting cross-country HIFs in distribution networks. The proposed method was effective in identifying this type of fault under various conditions, including capacitor bank switching, load switching, feeder energization, and unbalanced load. Unlike complex approaches, this technique analyzes voltage signals at a single monitoring point and performs correlation operations with those signals in typical scenarios. The identification of the faulty phase during cross-country HIFs relies on just three features extracted from the cross-correlogram of voltage signals. To streamline the feature extraction process, a cross-correlation-based method was used, which helps mitigate the impact of random uncorrelated noise in the signal. The slime mould optimization technique was used to determine the optimal monitoring point locations to identify the faulty bus in the network. The efficiency of the proposed method was verified on a real-time platform, and its simplicity was highlighted by its lack of reliance on distributed parameters, artificial intelligence techniques, or time synchronization with monitoring devices.

REFERENCES

[1]   F. M. Gatta, A. Geri, S. Lauria, M. Maccioni, A. Cerretti, and L. D'Orazio, "Large Temporary Overvoltages in MV Network due to a Series Fault in the HV Subtransmission System," in *2021 IEEE Madrid PowerTech*, Madrid, Spain, Jun. 2021, pp. 1–6, https://doi.org/10.1109/PowerTech46648.2021.9494822.

[2]   K. Solak and W. Rebizant, "Analysis of differential protection response for cross-country faults in transmission lines," in *2010 Modern Electric Power Systems*, Wroclaw, Poland, Sep. 2010.

[3]   A. A. M. Zin, N. A. Omar, A. M. Yusof, and S. P. A. Karim, "Effect of 132kV Cross-Country Fault on Distance Protection System," in *2012*

Sixth Asia Modelling Symposium, Bali, Indonesia, Feb. 2012, pp. 167–172, https://doi.org/10.1109/AMS.2012.17.

[4] Z. Y. Xu, W. Li, T. S. Bi, G. Xu, and Q. X. Yang, "First-Zone Distance Relaying Algorithm of Parallel Transmission Lines for Cross-Country Nonearthed Faults," *IEEE Transactions on Power Delivery*, vol. 26, no. 4, pp. 2486–2494, Jul. 2011, https://doi.org/10.1109/TPWRD.2011.2158455.

[5] T. Bi, W. Li, Z. Xu, and Q. Yang, "First-Zone Distance Relaying Algorithm of Parallel Transmission Lines for Cross-Country Grounded Faults," *IEEE Transactions on Power Delivery*, vol. 27, no. 4, pp. 2185–2192, Jul. 2012, https://doi.org/10.1109/TPWRD.2012.2210740.

[6] S. R. Kumar Joga, P. Sinha, M. K. Maharana, C. Jena, A. Mishra, and A. Roy, "Stockwell Transform and Data Mining based Fault Diagnosis Method to protect Microgrid," in *2022 3rd International Conference for Emerging Technology (INCET)*, Belgaum, India, Feb. 2022, pp. 1–5, https://doi.org/10.1109/INCET54531.2022.9824471.

[7] S. R. K. Joga, P. Sinha, and M. K. Maharana, "A novel graph search and machine learning method to detect and locate high impedance fault zone in distribution system," *Engineering Reports*, vol. 5, no. 1, 2023, Art. no. e12556, https://doi.org/10.1002/eng2.12556.

[8] S. AsghariGovar and H. Seyedi, "Adaptive CWT-based transmission line differential protection scheme considering cross-country faults and CT saturation," *IET Generation, Transmission & Distribution*, vol. 10, no. 9, pp. 2035–2041, 2016, https://doi.org/10.1049/iet-gtd.2015.0847.

[9] S. Singh and D. N. Vishwakarma, "A Novel Methodology for Identifying Cross-Country Faults in Series-Compensated Double Circuit Transmission Lines," *Procedia Computer Science*, vol. 125, pp. 427–433, Jan. 2018, https://doi.org/10.1016/j.procs.2017.12.056.

[10] A. Swetapadma and A. Yadav, "An artificial neural network-based solution to locate the multilocation faults in double circuit series capacitor compensated transmission lines," *International Transactions on Electrical Energy Systems*, vol. 28, no. 4, 2018, Art. no. e2517, https://doi.org/10.1002/etep.2517.

[11] V. Ashok and A. Yadav, "A Protection Scheme for Cross-Country Faults and Transforming Faults in Dual-Circuit Transmission Line Using Real-Time Digital Simulator: A Case Study of Chhattisgarh State Transmission Utility," *Iranian Journal of Science and Technology, Transactions of Electrical Engineering*, vol. 43, no. 4, pp. 941–967, Dec. 2019, https://doi.org/10.1007/s40998-019-00202-w.

[12] V. Ashok, A. Yadav, and A. Y. Abdelaziz, "MODWT-based fault detection and classification scheme for cross-country and evolving faults," *Electric Power Systems Research*, vol. 175, Oct. 2019, Art. no. 105897, https://doi.org/10.1016/j.epsr.2019.105897.

[13] A. Nikander and P. Järventausta, "Identification of High-Impedance Earth Faults in Neutral Isolated or Compensated MV Networks," *IEEE Transactions on Power Delivery*, vol. 32, no. 3, pp. 1187–1195, Jan. 2017, https://doi.org/10.1109/TPWRD.2014.2346831.

[14] B. Kumar and A. Yadav, "Backup protection scheme for transmission line compensated with UPFC during high impedance faults and dynamic situations," *IET Science, Measurement & Technology*, vol. 11, no. 6, pp. 703–712, 2017, https://doi.org/10.1049/iet-smt.2016.0458.

[15] O. E. Batista, R. A. Flauzino, M. A. de Araujo, L. A. de Moraes, and I. N. da Silva, "Methodology for information extraction from oscillograms and its application for high-impedance faults analysis," *International Journal of Electrical Power & Energy Systems*, vol. 76, pp. 23–34, Mar. 2016, https://doi.org/10.1016/j.ijepes.2015.09.019.

[16] B. K. Ponukumati, P. Sinha, M. K. Maharana, A. V. P. Kumar, and A. Karthik, "An Intelligent Fault Detection and Classification Scheme for Distribution Lines Using Machine Learning," *Engineering, Technology & Applied Science Research*, vol. 12, no. 4, pp. 8972–8977, Aug. 2022, https://doi.org/10.48084/etasr.5107.

[17] B. K. Ponukumati, P. Sinha, M. K. Maharana, C. Jenab, A. V. Pavan Kumar, and K. Akkenaguntla, "Pattern Recognition Technique Based Fault Detection in Multi-Microgrid," in *2021 IEEE 2nd International Conference on Applied Electromagnetics, Signal Processing, & Communication (AESPC)*, Bhubaneswar, India, Nov. 2021, pp. 1–6, https://doi.org/10.1109/AESPC52704.2021.9708541.

[18] B. K. P, P. Sinha, M. K. Maharana, C. Jena, A. V. Pavan Kumar, and K. Akkenaguntla, "Power System Fault Detection Using Image Processing And Pattern Recognition," in *2021 IEEE 2nd International Conference on Applied Electromagnetics, Signal Processing, & Communication (AESPC)*, Bhubaneswar, India, Nov. 2021, pp. 1–5, https://doi.org/10.1109/AESPC52704.2021.9708475.

[19] P. Ilius, M. Almuhaini, M. Javaid, and M. Abido, "A Machine Learning–Based Approach for Fault Detection in Power Systems," *Engineering, Technology & Applied Science Research*, vol. 13, no. 4, pp. 11216–11221, Aug. 2023, https://doi.org/10.48084/etasr.5995.

[20] B. Dhouib, M. A. Zdiri, Z. Alaas, and H. H. Abdallah, "Analyzing the Effects of MBPSS on the Transit Stability and High-Level Integration of Wind Farms during Fault Conditions," *Engineering, Technology & Applied Science Research*, vol. 13, no. 3, pp. 10652–10658, Jun. 2023, https://doi.org/10.48084/etasr.5838.

[21] P. Balamurali Krishna and P. Sinha, "Detection of Power System Harmonics Using NBPSO Based Optimally Placed Harmonic Measurement Analyser Units," in *2018 Second International Conference on Computing Methodologies and Communication (ICCMC)*, Erode, India, Feb. 2018, pp. 369–373, https://doi.org/10.1109/ICCMC.2018.8488114.

[22] Y. Xue, X. Chen, H. Song, and B. Xu, "Resonance Analysis and Faulty Feeder Identification of High-Impedance Faults in a Resonant Grounding System," *IEEE Transactions on Power Delivery*, vol. 32, no. 3, pp. 1545–1555, Jun. 2017, https://doi.org/10.1109/TPWRD.2016.2641045.